Nanoscale

Kinetic trapping of nanoparticles by solvent-induced interactions

Journal:	*Nanoscale*
Manuscript ID	NR-ART-12-2023-006469
Article Type:	Paper
Date Submitted by the Author:	18-Dec-2023
Complete List of Authors:	Colosqui, Carlos; Stony Brook University, Mechanical Engineering Takeuchi, Kenneth; Stony Brook University, Chemistry Takeuchi, Esther; Stony Brook University, Materials Science and Engineering Marschilok, Amy; Stony Brook University, Materials Science and Engineering Drazer, German; Rutgers, The State University of New Jersey, Mechanical and Aerospace Engineering Singletary, Troy; Stony Brook University, Mechanical Engineering

Journal Name

ARTICLE TYPE

Cite this: DOI: 00.0000/xxxxxxxxxx

Kinetic trapping of nanoparticles by solvent-induced interactions†

Troy Singletary,[a] German Drazer,[b] Amy C. Marschilok,[c,d,e,f] Esther S. Takeuchi,[c,d,e,f] Kenneth J. Takeuchi,*[c,d,e,f] Carlos E. Colosqui,*[a,f]

Received Date
Accepted Date

DOI: 00.0000/xxxxxxxxxx

Theoretical analysis based on mean field theory indicates that solvent-induced interactions (i.e. structural forces induced by the rearrangement of wetting solvent molecules) not considered in DLVO theory can induce the kinetic trapping of nanoparticles at finite nanoscale separations from a well-wetted surface, under a range of ubiquitous physicochemical conditions for inorganic nanoparticles of common materials (e.g., metal oxides) in water or simple molecular solvents. This work proposes a simple analytical model that is applicable to arbitrary materials and simple solvents to determine the conditions for direct particle-surface contact or kinetic trapping at finite separations, by using experimentally measurable properties (e.g., Hamaker constants, interfacial free energies, and nanoparticle size) as input parameters. Analytical predictions of the proposed model are verified by molecular dynamics simulations and numerical solution of the Smoluchowski diffusion equation.

Introduction

Predicting the conditions that would result in direct contact and physical adhesion of nanoparticles to a solid surface in liquid media is critical for numerous nanotechnology applications such as self-assembly of nanomaterials[1–5], membrane-based separation and nanofiltration[6–8], colloidal stabilization,[9–12] and enhancing charge transfer at electrode-electrolyte interfaces,[13–17] among many others. Furthermore, the physical adhesion of nanoparticles is an essential process in the hetero- or homoaggregation of nanoparticles and its better understanding is critical to develop accurate models for the environmental fate and toxicity of nanomaterials that are extensively used in industrial applications.[18–20]

The conventional analytical approach for modeling physical adhesion and aggregation of nanoparticles in liquid media is currently based on the classical Derjaguin-Landau-Verwey-Overbeek (DLVO) theory, which considers van der Waals (vdW) and electrostatic interactions by assuming a perfectly uniform solid and liquid medium (e.g., constant number density and permittivity in the solid and liquid media).[21–23] However, at nanoscale distances from a solid-liquid interface the wetting liquid is strongly non-uniform and anisotropic with large spatial variations of the local number density and/or permittivity induced by molecular-level structures (e.g., hydration or solvation shells) with quasi-crystalline order, anisotropic dipole orientation, and hydrogen bond networks.[24–27] The re-arrangement of these molecular structures, and the corresponding changes in free energy, when two wetted surfaces approach contact gives rise to so-called solvent-induced interactions, of which the oscillatory structural force and attractive/repulsive hydrophobic and hydrophilic forces are among the most notorious examples.[24,28–30] It is well established that such type of solvent-induced interactions not considered in DLVO theory can dominate the near-contact dynamics of planar surfaces in liquid.[23,31–33]

DLVO theory with the conventional assumption of a perfectly uniform solid and liquid medium provides effective analytical expressions to prevent nanoparticle contact and aggregation from the empirical or theoretical knowledge of (1) Hamaker constants A parameterizing vdW forces and (2) the surface zeta potential ζ (or diffuse-layer potentials) to determine the Electric Double Layer (EDL) force at a given pH and ionic strength I.[34–37] Substantial limitations must be expected when considering solely DLVO interactions to predict the equilibrium and dynamic conditions under which particle-surface contact in liquid media is attained. At single-digit nanometer separation between wetted surfaces, the change in free energy can present multiple local minima and long-lived metastable states induced by solvent-induced

[a] Mechanical Engineering Department, Stony Brook University, Stony Brook, NY 11794, USA
[b] Mechanical and Aerospace Engineering Department, Rutgers University, NJ 08854
[c] Department of Chemistry, Stony Brook University, Stony Brook, NY 11794
[d] Interdisciplinary Science Department, Brookhaven National Laboratory, Upton, NY 11973
[e] Department of Materials Science and Chemical Engineering, Stony Brook University, Stony Brook, NY 11794
[f] The Institute of Energy: Sustainability, Environment, and Equity, Stony Brook University, NY 11794
* E-mail: kenneth.takeuchi.1@stonybrook.edu; carlos.colosqui@stonybrook.edu

† Electronic Supplementary Information (ESI) available: See DOI: 00.0000/00000000.

interactions that are not considered in DLVO theory.[23,38–41] Furthermore, it is well-established that DLVO predictions alone cannot account for the interfacial surface energy γ associated with the degree of wettability of a surface and readily determined experimentally from the reversible work $W = -2\gamma A_c$ required to bring two wetted surfaces into direct contact over a finite contact area A_c. It is worth noting here that the solid-liquid interfacial surface energy γ is negative in the case of wettable surfaces for which liquid molecules reduce the free energy through contact with the solid surface;[42] the equilibrium contact angle for such surfaces is less than 90 deg. according to Young's law.[43–45]

This work proposes a compact mean-field model that considers solvent-induced interactions in order to accurately predict physicochemical and dynamic conditions under which nanoparticle contact and physical adhesion is attained or prevented. The proposed model including solvent-induced interactions predicts the kinetic trapping of nanoparticles at a finite rage of distances from the liquid-solid interface for critically low values of the Hamaker constant (i.e., for critically weak vdW attraction) or high values of the interfacial surface energy (i.e., for wettable surfaces). To verify the modeling assumptions and analytical predictions we perform numerical solution of the time-dependent Smoluchowski diffusion equation and molecular dynamics (MD) simulations for quasi-spherical nanoparticles of sizes between 2 and 4 nm near contact with a planar surface having well-controlled surface energies. The proposed mean-field model, Smoluchowski equation predictions, and MD simulations show good agreement and document a critical role of solvent-induced interactions by trapping nanoparticles at different metastable positions and controlling the time scales required to attain thermodynamic equilibrium at the particle-surface contact position.

Methods

Mean Field Theory We will consider that the potential of mean force (PMF) $U = U_{DLVO} + U_S$ for a nanoparticle in liquid media is composed of two contributions: (i) U_{DLVO} from conventional DLVO interactions in perfectly homogeneous media and (ii) U_S from solvent-induced interactions due to reconfiguration of the molecular liquid structure. For a spherical nanoparticle of radius R and a planar wall, the PMF $U = U(d)$ can be parameterized by the separation distance d between the particle-liquid the wall-liquid interface located at the wall-normal coordinate $y = y_w$ (see Fig. 1a). In this mean-field description for which the particle-liquid and wall-liquid interfaces are sharp (i.e., interfaces have zero thickness), particle-wall contact is virtual and occurs at a zero-dimensional point for which $d = 0$. We will consider that physical contact actually occurs over a finite contact area $A_c = \pi R_c^2$ defined by the effective contact radius R_c, as illustrated in Fig. 1a.

Due to spatial oscillations of the PMF resulting from solvent-induced interactions and the nanoscale interfacial topography, stable physical adhesion can occur at a finite separation distance d_0 for which $U(d_0) = \min(U)$ is the global energy minimum, as illustrated in Fig. 1b. The exact value of the stable adhesion distance d_0 is highly specific to the particular physicochemical conditions (e.g., surface energies magnitude and sign, Hamaker constant and ionic strength) and the molecular structure (e.g., crystalline lattice type) and nanoscale topography of the nanoparticle and wall surfaces (e.g., particle shape and faceting, nanoscale surface roughness). Metastable adhesion is expected at a finite set of distances $d_n \simeq d_0 + n\sigma \quad (n = 1, N_d)$ (see Fig. 1b) for which the PMF $U(d)$ has local minima with a period comparable to the characteristic liquid molecule diameter σ; such an energy profile is typically produced by oscillatory structural forces.[24,28,30,32,41]

We will focus this analysis on the case of attractive particle-wall vdW interactions ($A \geq 0$) and wettable surfaces ($\gamma < 0$) under near-contact conditions for which vdW forces dominate over electrostatic EDL forces (i.e. $\partial U_{vdw}/\partial d \gg \partial U_{EDL}/\partial d$) and thus $U_{DLV0} \simeq -AR/(6d')$, where the shifted distance $d' = d + \sigma/2$ accounts for a finite-size repulsive core prescribed by the molecular diameter. The studied conditions correspond to nanoscale separation distances smaller than a critical value $d^* = (A/k_BT)^{1/2} \times (12\pi n_0 \lambda_D)^{-1/2}$, where k_B is the Boltzmann constant, T is the system temperature, n_0 is the ion number density in the liquid bulk, and λ_D is the Debye screening length for the corresponding ionic strength in an electroneutral system. For reference, $d^* \simeq 3$ to 9 nm for a Hamaker constant $|A| = 5k_BT$ and a symmetric 1:1 electrolyte in aqueous solution at concentrations between $n_0 = 0.1$ and 10 mM. We further consider that the oscillatory structural force associated to molecular layering is the dominant contribution from solvent-induced interactions for the studied near-contact conditions (i.e., for $d \lesssim$ 10-15 σ).[24,28,30,32,41]

We therefore adopt the heuristic expression for plane surfaces[23,30,46] $U_S = U_w \exp(-d/\sigma)\cos(2\pi d/\sigma)$ parameterized by the "wetting" energy $U_w = U_S(0)$ required to remove the liquid separating the surfaces.

Potential of Mean Force Considering DLVO and solvent-induced interactions for the studied near-contact conditions, the nanoparticle PMF is modeled as

$$U(d) = -\frac{AR}{6d'} + U_w e^{-\frac{d}{\sigma}} \cos\left(\frac{2\pi d}{\sigma}\right). \qquad (1)$$

The functional form of the PMF in Eq. 1 with multiple local minima is illustrated in Fig. 1b. It is worth noting that modeling solvent-induced interactions as a harmonic spatial oscillation of period σ ceases to be a valid approximation for $d \leq \sigma$, i.e., at separations below one molecular diameter for which the particle becomes partially inserted in the first solvation layer (see Fig. 1b). Moreover, the separation for stable contact does not necessarily correspond to the global minimum predicted at $d_0 \simeq \sigma/2$ by Eq. 1 and is specific to the nanoscale surface topography and interfacial surface energy value, as discussed above.

To complete the PMF formulation in Eq. 1 we consider that the contact energy solely due to solvent-induced interactions, $U_w = -2\bar{\gamma}\pi R_c^2$, is determined by the average interfacial energy $\bar{\gamma} = (\gamma_1 + \gamma_2)/2$, where $\gamma_i \quad (i = 1,2)$ are the interfacial energies of the particle-liquid and wall-liquid interfaces. To estimate the effective contact radius for a quasi-spherical nanoparticle we propose the simple expression $R_c = R\sqrt{1-(1-\delta/R)^2}$ with $\delta \simeq \sigma$, so that the contact radius is determined from the area removed from the first solvation layer when particle-wall contact is attained (cf. Fig. 1a). The solid-liquid interfacial energy γ_i will be treated as a

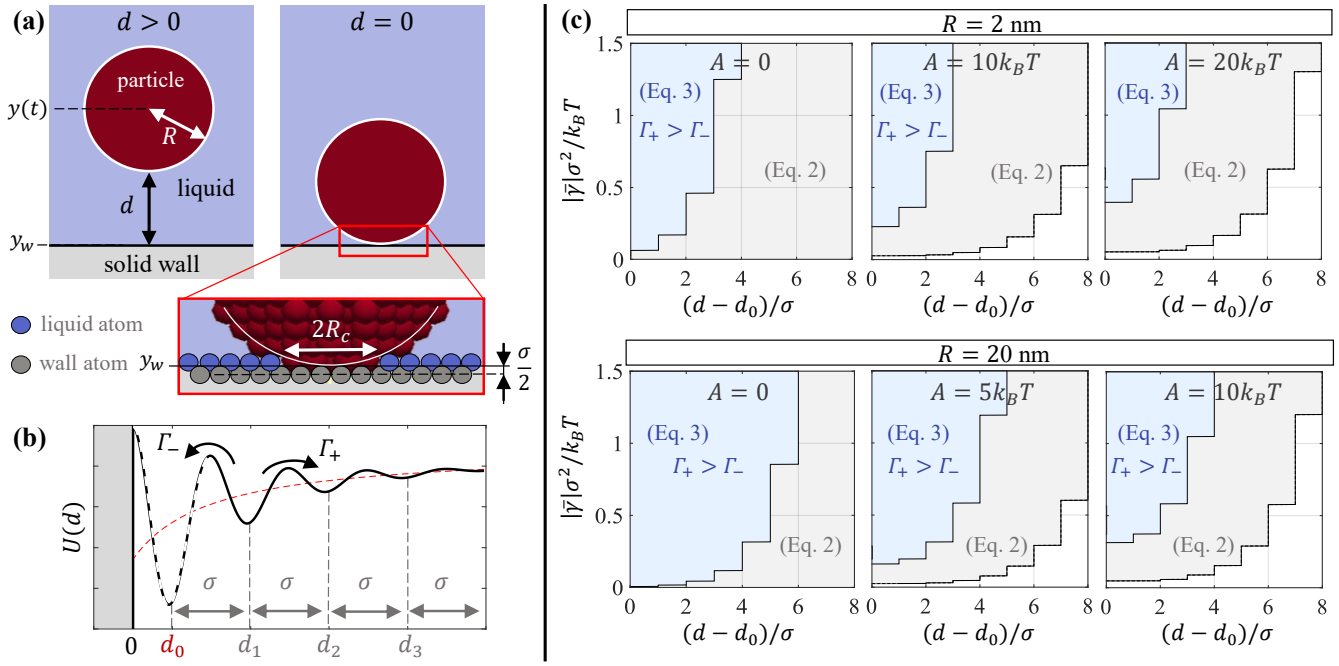

Fig. 1 Solvent-induced interactions and kinetic trapping. (a) Approach and contact of a spherical nanoparticle to plane wall immersed in liquid characterized by the separation distance $d \geq 0$. The finite contact radius R_c is prescribed by the characteristic atomic diameter σ. (b) The nanoparticle PMF $U = U_{DLVO} + U_S$ modeled by Eq. 1 (solid black line) has periodic minima at distances d_i (the red dashed line represents U_{DLVO}). The stable contact distance d_0 and functional form of the PMF for $d \leq \sigma$ (dashed black line) is highly specific to the nanoscale interfacial topography and physicochemical conditions. (c) Kinetic trapping and metastability conditions at discrete particle-wall separations for a nanoparticle of radius $R = 2$ nm & 20 nm, Hamaker constant $A = 0$, 10, & 20 k_BT, and interfacial energy magnitudes $|\bar{\gamma}| \leq 1.5 k_BT/\sigma^2$. Gray shaded area: wall-particle separations satisfying the metastability condition in Eq. 2. Blue shaded area: wall-particle separations for which $\Gamma_+ \geq \Gamma_i$ according to Eq. 3, kinetic trapping occurs at the outer boundary.

material property determinable from experimental measurements or analytical means for two plane surfaces. The validity of the modeling assumptions leading to Eq. 1 will be assessed by comparison of theoretical predictions with MD simulation results.

Metastable adhesion The solvent-induced interactions considered in Eq. 1 produce multiple energy minima for a finite set of nearly periodic distances $d_n \simeq d_0 + n\sigma$ (cf. Fig. 1b) that satisfy the condition

$$e^{-\frac{d_n}{\sigma}} \left(\frac{d_n}{\sigma} + \frac{1}{2} \right)^2 \geq \frac{|A|}{|\bar{\gamma}|\sigma^2} \times \left(\frac{R\sigma}{24\pi^2 R_c^2} \right). \qquad (2)$$

The expression in Eq. 2 uses the estimate $\sqrt{1+4\pi^2} \simeq 2\pi$. Predictions from Eq. 2 are reported in Fig. 1c for a range of typical values of (attractive) Hamaker constants ($A = 0$, 10, and 20 k_BT) and interfacial surface energy magnitudes ($|\gamma| \leq 1.5\ k_BT/\sigma^2$) for a spherical nanoparticle of radius $R = 2$ and 20 nm. Metastable adhesion occurs at finite separations from the wall for weak particle-wall attraction and/or large magnitude of the interfacial surface energies (cf. Fig. 1c). Substantial deviations from Brownian diffusion and DLVO theory predictions, with a significantly hindered contact dynamics, are expected under conditions for which Eq. 2 is satisfied and multiple metastable states exist at finite separations d_n from the wall.

According to Eq. 2, mestastable adhesion occurs for Hamaker constant magnitudes smaller than a critical value $A_m = 67.3|\bar{\gamma}|\pi R_c^2 \sigma/R$, for which there is only a metastable state at the closest local minima from the wall $d_1 = d_0 + \sigma$. For the case of quasi-spherical particles of radius much larger than the liquid molecule diameter $R \gg \sigma$ and with a finite contact radius $R_c = R\sqrt{2\sigma/R}$ (see Fig. 1a), Eq. 2 predicts a (size-independent) Hamaker constant magnitude $A_m \simeq 422.82|\bar{\gamma}|\sigma^2$, above which metastability is completely prevented and solely considering DLVO interactions can describe accurately the contact dynamics. This analysis thus predicts that exceptionally large Hamaker constants, $|A| > A_m =$ 200-400 k_BT, are required to prevent metastable adhesion for the case of conventional hydrophilic surfaces in water for which $|\bar{\gamma}| =$ 0.5-1 k_BT/σ^2 (e.g., common metal oxides and polymer surfaces).

Kinetic trapping When the particle is near a metastable position d_n with neighboring maxima in the forward/backward directions (+/−) at $d_\pm = d_n \pm \sigma/2$ and thus $|d - d_n| \leq \sigma/2$, one can assume a probability distribution $p(d,t) \propto \exp(-U/k_BT)$ that is approximately governed by a diffusion equation with constant translational diffusivity D. Hence one can estimate the characteristic diffusive times $T_\pm(d_n) = k_BT/(D\ddot{U}_\pm) \times \exp(\Delta U_\pm/k_BT)$ for crossing over the forward/backward maxima; here, $\ddot{U}_\pm \equiv \ddot{U}(d_\pm)$ is the PMF second-order derivative at the corresponding neighboring maxima and $\Delta U_\pm = U(d_\pm) - U(d_n)$ are the energy barriers separating neighboring metastable states in the forward/backward directions. At metastable separation distances d_n, for which Eq. 2 is satisfied, the nanoparticle approach to the surface is approxi-

mately described by a rate equation $\dot{d} = \sigma \times (\Gamma_+ - \Gamma_-)$ with forward/backward rates $\Gamma_\pm = 1/T_\pm$.

The "kinetic" trapping of the particle will occur when $\Gamma_+ \geq \Gamma_-$ and the particle-wall separation $d(t)$ cannot be further reduced by biased thermally activated transitions between metastable states. The kinetic trapping thus occurs at the farthest metastable separation $d_n = d_0 + n\sigma$ for which

$$U(d_n - \sigma/2) - U(d_n + \sigma/2) - k_B T \geq 0. \quad (3)$$

Predictions from Eq. 3 employing the PMF $U(d)$ modeled in Eq. 1 are reported in Fig. 1c, along with the conditions for satisfying metastability (Eq. 2), for a range of conditions commonly encountered for nanoparticles of conventional metal oxides [9,35,47,48] (e.g., Fe3O4, SiO2, TiO2) or polymeric materials. [49–51] For wettable substrates with $|\bar{\gamma}| \sim k_B T/\sigma^2$, the kinetic trapping can occur farther than four molecular layers away from the wall (i.e., $d \gtrsim 1$ nm) (cf. Fig. 1c).

Critical conditions for contact The model in Eqs. 1-3 can estimate the conditions for which particle-wall contact is possible by considering the nanoparticle shape and surface wettability. Particle-wall contact requires avoiding kinetic trapping at the local minima $d_1 = d_0 + \sigma/2$ closest to the wall, which according to Eq. 3 is expected for Hamaker constants above a critical value

$$A_c = \left(0.465\pi R_c^2 |\bar{\gamma}| - k_B T\right) \times (22.5\sigma/R), \quad (4)$$

prescribed by the particle radius, contact area, and interfacial surface energies of the particle-liquid and wall-liquid interfaces. It is worth noting that Eq. 4 provides conservative estimates for the attractive vdW forces needed to attain contact by solely considering translational motion normal to the wall.

Hence, according to Eq. 4, a "large" quasi-spherical nanoparticle with $R \gg \sigma$ and $R_c \simeq R\sqrt{2\sigma/R}$ will attain contact for Hamaker constants larger than the critical value $A_c = 65.7|\bar{\gamma}|\sigma^2$. As noted in the previous section for the case of hydrophilic surface and nanoparticle materials in aqueous solution, particle-wall contact and stable physical adhesion at $d = d_0$ requires rather large Hamaker constants $A \gtrsim$ 30-65 $k_B T$. Additionally, Eq. 4 predicts that contact and stable adhesion can still be attained for vanishingly small DLVO interactions with $A \simeq 0$, for sufficiently low magnitudes of the interfacial surface energy $|\bar{\gamma}| < 0.685 k_B T/R_c^2$ (cf. Fig. 1c). For a vanishingly small Hamaker constant $A \simeq 0$, contact areas $A_c \simeq \pi\sigma^2$ of molecular dimensions would be required to attain particle-wall contact for a hydrophilic particle and/or wall surface.

Results and discussion

To assess the validity of the proposed mean-field model in Eqs 1-4, we perform (1) numerical solution of the Smoluchowski diffusion equation and (2) MD simulations for the contact dynamics for quasi-spherical nanoparticles on a planar wall with different interfacial surface energies. The employed mesoscale and atomistic models report the time-dependent rms distance, which enables direct verification of analytical predictions for the kinetic trapping of nanoparticles and contact conditions.

Smoluchowski diffusion equation The mesoscale description of the contact dynamics is based on the time-dependent probability density function $p(y,t)$ for the center-of-mass position of the nanoparticle along the y-direction normal to a plane wall located at $y = y_w$ (cf. Fig. 1a). Assuming overdamped Brownian motion with uniform thermal energy $k_B T$, the evolution of the probability density $p(y,t)$ is governed by the Smoluchowski diffusion equation

$$\frac{\partial}{\partial t} p(y,t) = \frac{\partial}{\partial y}\left[D e^{-\frac{U}{k_B T}} \frac{\partial}{\partial y} e^{\frac{U}{k_B T}} p(y,t) \right], \quad (5)$$

where D is the nanoparticle translational diffusivity, and the PMF $U(d)$ defined in Eq. 1 is parameterized by the separation distance $d = y_w - R - y$. Eq. 5 is solved numerically for $0 \leq y \leq y_w$ with zero-flux boundary conditions $\frac{\partial}{\partial y}[e^{U/k_B T} p(y,t)] = 0$ at $y = 0$ and $y = y_w$. The nanoparticle diffusivity D is estimated from the constant free-space diffusivity, considering that hindrance to the contact dynamics is largely caused by solvent-induced interactions rather than near-wall hydrodynamic friction; the validity of this approximation is examined by comparison with MD simulations.

For a nanoparticle of radius R with an initial center-of-mass position $y(0) = 0$ we define the root-mean-square (rms) displacement normal to the wall $\bar{y}(t) = \left[\int_0^{y_w} p(y,t) y^2 dy\right]^{1/2}$ and thus the rms separation distance

$$\bar{d}(t) = y_w - R - \bar{y}(t). \quad (6)$$

Far from the wall, where $U(d) \simeq 0$, Eq. 5 gives the conventional expressions for free-space Brownian motion $p(y,t) = (4\pi D t)^{-1/2} \exp(-y^2/(4Dt))$ and Eq. 6 gives $\bar{d} = y_w - R - \sqrt{2Dt}$. We therefore define the diffusive time $T_D = (y_w - R)^2/(2D)$ as a characteristic time scale for nanoparticle-wall contact.

Molecular dynamics Atomistic simulations considering pairwise DLVO interactions are instrumental to verify the predictions in Eqs. 1-3 based on the PMF $U(d)$ formulated for considering solvent-induced interactions. For this purpose we perform fully atomistic MD simulations of the physical adhesion of a single quasi-spherical nanoparticle onto a plane wall fully immersed in a liquid (see Fig. 2a) using the open-source package LAMMPS. [52] Our MD simulations employ standard 12-6 Lennard-Jones (L-J) potentials modeling hard-core and vdW pairwise interactions from which collective molecular-level interactions that control nanoparticle adhesion, including solvation and oscillatory structural forces and other solvent-induced interactions, arise dynamically. [53–55]

As reported in Fig. 2a, the nanoparticle (p), plane wall (w), and liquid solvent (l) are made of three different species having the same atomic diameter σ and mass m. A quasi-spherical nanoparticle of radius $R =$ 3 & 6 σ (i.e., 2 & 4 nm diameter) is carved out of a fcc lattice with uniform spacing $\Delta x = 4^{1/3}\sigma$ and the plane wall is a "frozen" fcc lattice with the same uniform spacing Δx (cf. Fig. 2a). The particle and wall number densities $n_p = n_w = 1/\sigma^3$ are thus uniform and equal. The simulation domain (see Fig. 2a) is a 3D periodic box fully filled with the liquid and confined along the y-direction by the wall. The average number density of the liquid is $n_l = 0.8/\sigma^3$. The pairwise L-J interactions between species are parameterized to produce three different solid-liquid interfa-

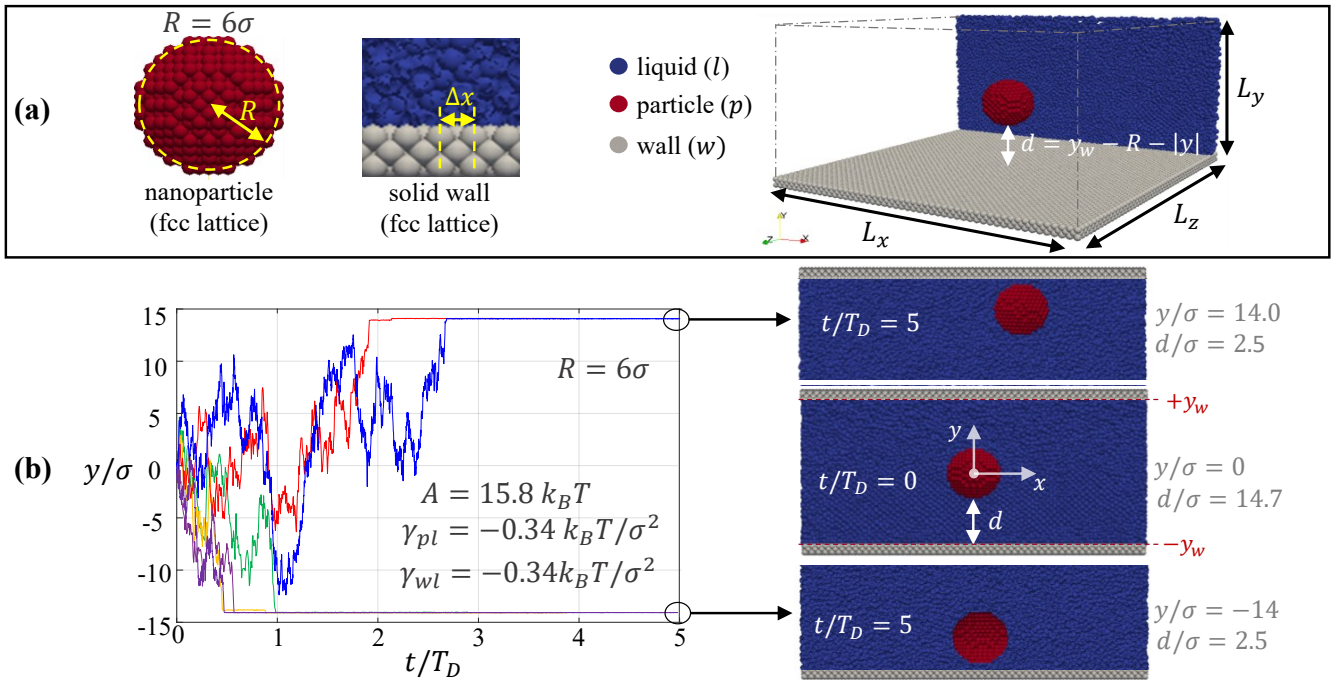

Fig. 2 Molecular dynamics simulations of nanoparticle contact. (a) Atomistic representation of the modeled quasi-spherical nanoparticle and solid wall, and periodic simulation domain ($L_x = 80\sigma$, $L_y = 42.5\sigma$, $L_z = 80\sigma$) that is fully filled with liquid. The particle-wall distance $d = y_w - R - |y|$ to the top/bottom walls located at $y = \pm y_w$ is computed from the center-of-mass normal coordinate $y(t)$ reported by MD simulations. (b) Replica MD simulations (colored lines) report different center-of-mass trajectories $y(t)$ for the same studied macroscopic initial condition and set of physical parameters. The cases reported correspond to $R = 6\sigma$, $A = 15.8 k_BT$, and $\gamma_{pl} = \gamma_{wl} = -0.34 k_BT/\sigma^2$.

cial energies γ = -0.23, -0.34, & -0.6 k_BT/σ^2 and three Hamaker constants $A \simeq 0$, 5, 10 k_BT for the particle-wall vdW interaction in the model liquid solvent. The MD force field parameterization and procedure to determine the interfacial surface energy is described in detail in the ESI.

To determine the rms separation distance $\bar{d}(t)$ (Eq. 6) we compute $y_{rms}(t) = (\sum_i^N y_i^2/N)^{1/2}$ with $N = 5$ replicas of each studied physical condition (cf. Fig. 2b) that are initialized with different atomic positions and velocities producing a macroscopically quiescent liquid with the targeted system temperature $T = 300$ K. Each replica simulation (Fig. 2b) is initialized with the nanoparticle at the center of the simulation domain and run over a time interval $T_s \simeq 5T_D$ corresponding to nearly 5 diffusive times. While the simulation time is sufficiently large so that the nanoparticle reaches within three atomic layers from the wall in every simulation, adhesion at finite distance from the wall or contact (either at the top or bottom side) are observed as probabilistic events (cf. Fig. 2b) with a likelihood prescribed by the surface energies of the particle-liquid (γ_{pl}) and wall-liquid (γ_{wl}) interfaces and the Hamaker constant for particle-wall interactions.

Nanoparticle near-contact dynamics Analytical predictions for the transition to metastable dynamics (Eq. 2) and kinetic trapping at finite separations $d_n > d_0$ (Eq. 3) are compared in Figs. 3-4 with the Smoluchowski equation and MD simulation results for the time-dependent rms separation from contact $\bar{d} - d_0$. The contact distance $d_0 = \sigma/2 \pm 20\%$ is determined from the MD simulations for which direct particle-wall contact is observed. The Smoluchowski equation with the PMF modeled in Eq. 1 and constant particle diffusivity, and MD simulation results are in reasonably good agreement under the studied conditions. Above the critical separation for metastability predicted by Eq. 2 the rms particle-wall separation predicted for pure Brownian motion with constant free-space diffusivity D is in close agreement with the Smoluchowski equation and MD simulations (cf. Fig. 3a & Fig. 4c).

The set of results in Fig. 3 correspond to the modeled quasi-spherical nanoparticle of radius $R = 6\sigma$, with moderately large Hamaker constants A = 7.9-23.7 k_BT and a set of nine different conditions with weak-to-moderate particle-liquid interfacial energies γ_{pl} = -0.6, -0.34, & -0.23 k_BT/σ^2 and wall-liquid interfacial energies γ_{wl} = -0.6, -0.34, & -0.23 k_BT/σ^2. The nine studied conditions are therefore characterized by only six different values of the average interfacial energy magnitude $|\bar{\gamma}| = |\gamma_{pl} + \gamma_{wl}|/2$ = 0.23-0.6 k_BT/σ^2 (cf. Fig. 3a-f). The conditions studied in Fig. 3 correspond to the case of an aqueous solution at room temperature, and moderately hydrophilic substrates with interfacial surface energies $\bar{\gamma} \simeq$ -37 to -10 mM/m^2 and (solid-water-air) Young contact angles $\theta_Y \simeq$ 60-80° that are reported for conventional metal oxide surfaces by different experimental techniques.[56–59] For the low interfacial energy magnitudes $|\bar{\gamma}| \lesssim 0.3 k_BT/\sigma^2$, the nanoparticles are able to eventually attain direct contact with the wall after crossing the metastable dynamics region predicted by Eq. 2 but they do so at substantially longer times than predicted for pure Brownian motion (cf. Fig. 3a-c). For critically large surface energies (cf. Fig. 3d-i) the kinetic trapping of the nanoparticle away from the wall is observed at the finite separations predicted by Eq. 3, and reported in Fig. 1c, with metastable separation

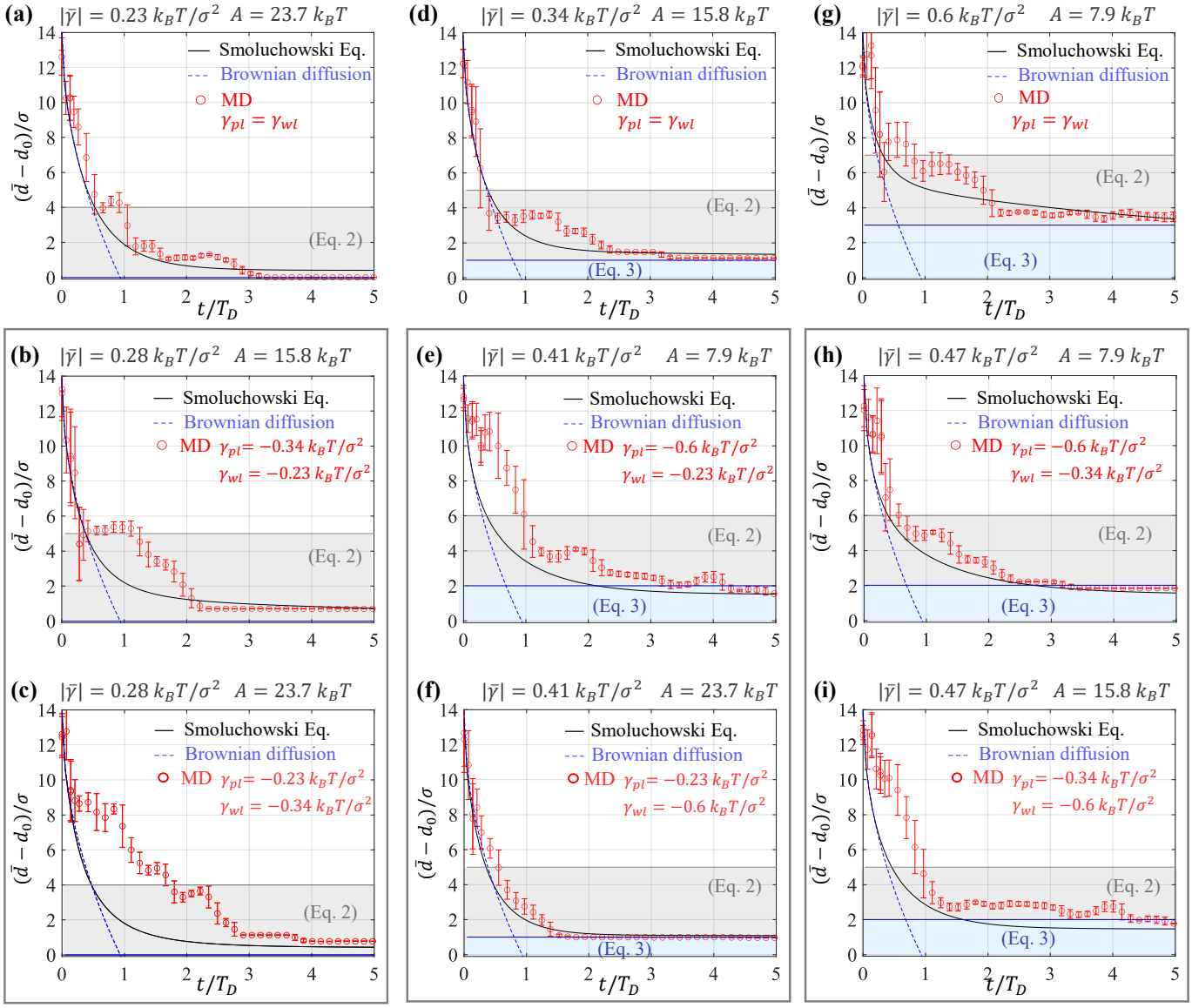

Fig. 3 Metastable contact dynamics and kinetic trapping. (a-f) Time-dependent rms separation $\bar{d}(t) - d_0$ from the contact position for a quasi-spherical nanoparticle of radius $R = 6\sigma$, for three Hamaker constants $A = 7.9$, 15.8, & 23.7 k_BT and six different values of the average interfacial energy magnitude $|\bar{\gamma}| = |\gamma_{pl} + \gamma_{wl}|/2 = 0.23\text{-}0.6 k_BT/\sigma^2$ (see figure labels) for nine different combinations of particle-liquid γ_{pl} and wall-liquid γ_{wl} interfacial energies (see legends). MD simulation results (markers) are compared with numerical solutions of the Smoluchwoski equation (Eq. 5) and analytical predictions for free-space Brownian motion (see legends). Grey shaded area: metastable dynamics region predicted by Eq. 2. Blue shaded area: region with $\Gamma_+ \geq \Gamma_-$ predicted by Eq. 3 with kinetic trapping predicted at the region boundary.

distances up to three liquid molecule diameters for the case of moderately wettable surfaces with an average interfacial energy $\bar{\gamma} \simeq -k_BT/\sigma^2$.

To further asses the validity of the analytical predictions for kinetic trapping and contact conditions in Eqs. 3-4, we perform an additional set of MD simulations for which the interfacial surface energy magnitude of the particle and wall $|\bar{\gamma}| = |\gamma_{pl}| = |\gamma_{wl}| = 0.34 k_BT/\sigma^2$ remains constant (with a moderate magnitude) as the Hamaker constant and nanoparticle radius is varied. The case reported in Fig. 4a corresponds to the condition modeled in Fig. 3d with a nanoparticle of radius $R = 6\sigma$ and $\gamma_{pl} = \gamma_{wl} = -0.34 k_BT/\sigma^2$, but with a vanishing Hamaker constant $A = 0$. Under this studied condition the particle becomes kinetically trapped at a finite separation of two molecular diameters from contact, due to solvent-induced interactions alone as predicted by Eq. 3 and reported in Fig. 1c for vanishing van der Waals forces between the particle and the wall.

The additional case in Fig. 4b corresponds to the same conditions reported in Fig. 3d, with $A \simeq 15.8\ k_BT$ and interfacial surface energies $\gamma_{pl} = \gamma_{wl} = -0.34 k_BT/\sigma^2$, but with a smaller nanoparticle of radius $R = 3\sigma$. As predicted via Eq. 4, we find that reducing the particle size, and thus the contact radius R_c, prevents the kinetic trapping at finite separations and direct particle-wall contact is observed (cf. Fig. 4b). The critical condition for contact in Eq. 4 is thus verified by MD simulations for the cases studied in Fig. 3 and Fig. 4 with small nanoparticles of radius $R \simeq 1$ to 2 nm and

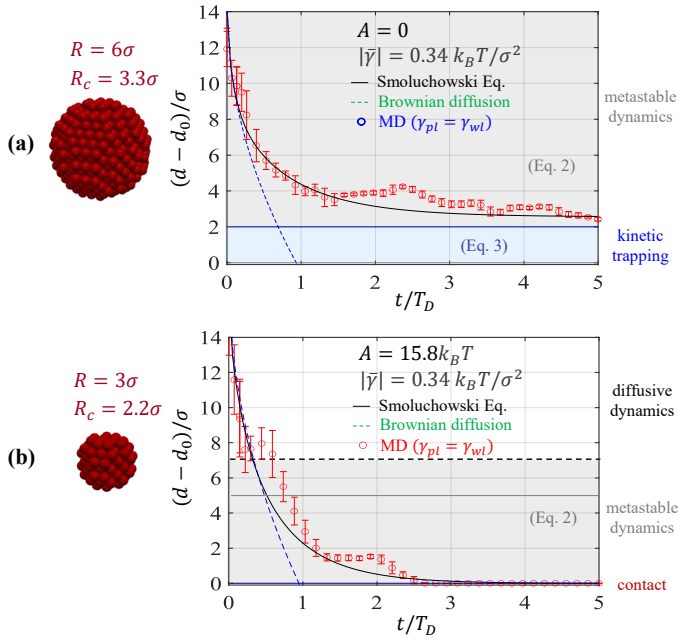

Fig. 4 Metastable contact dynamics and kinetic trapping: Time-dependent rms separation $\bar{d}(t) - d_0$ from contact for two cases with the same interfacial energy $|\bar{\gamma}| = |\gamma_{pl} + \gamma_{wl}|/2 = 0.34 k_BT/\sigma^2$ but different Hamaker constants and particle size. (a) $R = 6\sigma$ & $A = 0$. (b) $R = 3\sigma$ & $A = 15.8k_BT$. MD simulation results (markers) are compared with numerical solutions of the Smoluchowski equation (Eq. 5) and analytical predictions for free-space Brownian motion (see legends). Grey shaded area: metastable dynamics region predicted by Eq. 2. Blue shaded area: region with $\Gamma_+ \geq \Gamma_-$ predicted by Eq. 3 with kinetic trapping predicted at the region boundary.

a substantial variation of surface energy magnitudes $|\bar{\gamma}| = 0.23$-$0.6\ k_BT/\sigma^2$.

Conclusions

This work formulated and verified a mean-field model for predicting the conditions to attain or prevent the metastable adhesion and contact of nanoparticles to surfaces in liquid media by considering both conventional DLVO and solvent-induced interactions, the latter parameterized by the interfacial surface energy that prescribes the macroscale wetting properties of the nanoparticle and wall surfaces. The proposed simple model employs a compact set of experimentally measurable properties such as the interfacial surface energy and Hamaker constant and therefore can be applied to nanoparticles of arbitrary materials (e.g., crystalline or amorphous, polar/non-polar) and simple molecular solvents. The formulated model can predict the conditions for homo- and heteroaggregation of nanoparticles, colloidal stability of nanoparticle suspensions, or nanoparticle-electrode contact in liquid media with high electrolyte concentration and/or weak surface charge. The proposed model can be readily extended to include the electric double layer force when this is necessary.

A key prediction of the proposed model is the kinetic trapping of nanoparticles at finite nanoscale separations from contact for the case of moderately to highly hydrophilic materials (e.g., metal oxides, metals, and polymeric materials) dispersed in aqueous media. The predicted kinetic trapping at single-digit nanoscale separations from the wall leads to the effective prevention of particle-wall contact and has significant implications for understanding and controlling the contact and physical adhesion of nanoparticles to liquid-solid interfaces. This finding is particularly relevant to nanomaterials that are extensively employed in diverse technological and industrial applications, and are subsequently released in the environment.

The validity of the analytical predictions is verified by comparison with MD simulations studying quasi-spherical (crystalline) nanoparticles with vanishingly small to large attractive van der Waals interactions and a range of weakly to moderately wettable surfaces. For moderate to large magnitude of the interfacial surface energy, the analytical expression proposed for predicting the contact conditions accounts closely for MD simulation results and indicates that uncommonly large Hamaker constants are needed to fully prevent kinetic trapping and attain stable physical adhesion of small nanoparticles (i.e., smaller than 50 nm) at direct particle-wall contact. The findings of this work highlight the importance of considering solvent-induced interactions, prescribed by the surface wettability and nanoscale surface topography, to understand and ultimately control the adhesion, aggregation, and contact dynamics of small nanoparticles in liquid media and the faith of nanomaterials in the environment. In particular, the findings of this work provide valuable insights to understand mass and charge transport processes at liquid-solid interfaces that are mediated by the contact and physical adhesion of nanoparticles, macromolecules, and finite-size mass and charge carriers.

Conflicts of interest

There are no conflicts to declare.

Acknowledgements

Theoretical model development and validation analysis for this work were supported by the Center for Mesoscale Transport Properties, an Energy Frontier Research Center funded by the U.S. Department of Energy, Office of Science, Basic Energy Sciences, under award DE-SC0012673. T.S. acknowledges support from the National Science Foundation through award CBET-2016204 for performing MD simulations and numerical analysis.

Notes and references

1 R. Bhardwaj, X. Fang, P. Somasundaran and D. Attinger, *Langmuir*, 2010, **26**, 7833–7842.
2 V. Lotito and T. Zambelli, *Adv. Colloid Interface Sci.*, 2017, **246**, 217–274.
3 S. Srivastava, Z. A. Wahith, O. Gang, C. E. Colosqui and S. R. Bhatia, *Adv. Mater. Interfaces.*, 2020, **7**, 1901954.
4 S. H. Mejias, E. López-Martínez, M. Fernandez, P. Couleaud, A. Martin-Lasanta, D. Romera, A. Sanchez-Iglesias, S. Casado, M. R. Osorio, J. M. Abad *et al.*, *Nanoscale*, 2021, **13**, 6772–6779.
5 D. Gentili and G. Ori, *Nanoscale*, 2022, **14**, 14385–14432.
6 J. M. Dickhout, J. Moreno, P. Biesheuvel, L. Boels, R. Lammertink and W. De Vos, *J. Colloid Interface Sci.*, 2017, **487**, 523–534.

7 S. Al Aani, T. N. Mustafa and N. Hilal, *J. Water Process. Eng.*, 2020, **35**, 101241.

8 M. Enfrin, J. Wang, A. Merenda, L. F. Dumée and J. Lee, *J. Membr. Sci.*, 2021, **633**, 119379.

9 Y. Zhang, Y. Chen, P. Westerhoff, K. Hristovski and J. C. Crittenden, *Water Res.*, 2008, **42**, 2204–2212.

10 F. Gambinossi, S. E. Mylon and J. K. Ferri, *Adv. Colloid Interface Sci.*, 2015, **222**, 332–349.

11 A. Cardellini, M. Alberghini, A. G. Rajan, R. P. Misra, D. Blankschtein and P. Asinari, *Nanoscale*, 2019, **11**, 3979–3992.

12 A. Carone, S. Emilsson, P. Mariani, A. Désert and S. Parola, *Nanoscale Advances*, 2023, **5**, 2017–2026.

13 T. J. Anderson and B. Zhang, *Acc. Chem. Res.*, 2016, **49**, 2625–2631.

14 S. V. Sokolov, S. Eloul, E. Kätelhön, C. Batchelor-McAuley and R. G. Compton, *Phys. Chem. Chem. Phys.*, 2017, **19**, 28–43.

15 W. Xu, Y. Zhou and X. Ji, *J. Phys. Chem. Lett.*, 2018, **9**, 4976–4980.

16 S.-K. Jung, I. Hwang, D. Chang, K.-Y. Park, S. J. Kim, W. M. Seong, D. Eum, J. Park, B. Kim, J. Kim *et al.*, *Chem. Rev.*, 2019, **120**, 6684–6737.

17 C. R. Tang, L. M. Housel, C. Huang, W. Li, L. Wang, S. Yan, E. S. Takeuchi, A. C. Marschilok, C. E. Colosqui and K. J. Takeuchi, *J. Electrochem. Soc.*, 2022, **169**, 010519.

18 D. Lin, X. Tian, F. Wu and B. Xing, *J. Environ. Qual.*, 2010, **39**, 1896–1908.

19 K. L. Garner and A. A. Keller, *J. Nanopart Res.*, 2014, **16**, 1–28.

20 Y. Guo, N. Tang, J. Guo, L. Lu, N. Li, T. Hu, Z. Zhu, X. Gao, X. Li, L. Jiang *et al.*, *Chemosphere*, 2023, **310**, 136805.

21 N. V. Churaev, B. V. Derjaguin and V. M. Muller, *Surface forces*, Springer Science & Business Media, 2013.

22 J. Lyklema, *Fundamentals of interface and colloid science: soft colloids*, Elsevier, 2005, vol. 5.

23 J. N. Israelachvili, *Intermolecular and surface forces*, Academic press, 2011.

24 R. G. Horn and J. N. Israelachvili, *J. Chem. Phys.*, 1981, **75**, 1400–1411.

25 H.-J. Butt, M. Jaschke and W. Ducker, *Bioelectrochemistry*, 1995, **38**, 191–201.

26 Y. Chen, H. I. Okur, N. Gomopoulos, C. Macias-Romero, P. S. Cremer, P. B. Petersen, G. Tocci, D. M. Wilkins, C. Liang, M. Ceriotti *et al.*, *Sci. Adv.*, 2016, **2**, e1501891.

27 S. Shin and A. P. Willard, *J. Phys. Chem. B.*, 2018, **122**, 6781–6789.

28 J. Israelachvili, *Acc. Chem. Res.*, 1987, **20**, 415–421.

29 E. E. Meyer, K. J. Rosenberg and J. Israelachvili, *Proc. Natl. Acad. Sci. U.S.A.*, 2006, **103**, 15739–15746.

30 M. Ludwig and R. von Klitzing, *Curr. Opin. Colloid Interface Sci.*, 2020, **47**, 137–152.

31 R. M. Pashley and J. N. Israelachvili, *J. Colloid Interface Sci.*, 1984, **101**, 511–523.

32 J. N. Israelachvili and P. M. McGuiggan, *J. Mater. Res.*, 1990, **5**, 2223–2231.

33 S. O'shea and M. Welland, *Langmuir*, 1998, **14**, 4186–4197.

34 H. C. Hamaker, *physica, A.*, 1937, **4**, 1058–1072.

35 D. B. Hough and L. R. White, *Adv. Colloid Interface Sci.*, 1980, **14**, 3–41.

36 Z. Adamczyk and P. Weroński, *Adv. Colloid Interface Sci.*, 1999, **83**, 137–226.

37 D. Grasso*, K. Subramaniam, M. Butkus, K. Strevett and J. Bergendahl, *Rev. Environ. Sci. Biotechnol.*, 2002, **1**, 17–38.

38 Y. Liang, N. Hilal, P. Langston and V. Starov, *Adv. Colloid Interface Sci.*, 2007, **134**, 151–166.

39 C. A. Silvera Batista, R. G. Larson and N. A. Kotov, *Science*, 2015, **350**, 1242477.

40 S. Kumar, D. Saha, J. Kohlbrecher and V. K. Aswal, *Chem. Phys. Lett.*, 2022, **803**, 139808.

41 S. Huang, C. E. Colosqui, Y.-N. Young and H. A. Stone, *Soft Matter*, 2022, **18**, 4786–4791.

42 A. Mathur, P. Sharma and R. Cammarata, *Nat. Mater.*, 2005, **4**, 186–186.

43 T. Young, *Philos. Trans. Royal Soc. A.*, 1805, 65–87.

44 R. J. Good and L. A. Girifalco, *J. Phys. Chem. A*, 1960, **64**, 561–565.

45 T. Huhtamäki, X. Tian, J. T. Korhonen and R. H. Ras, *Nat. Protoc.*, 2018, **13**, 1521–1538.

46 P. A. Kralchevsky and N. D. Denkov, *Chem. Phys. Lett.*, 1995, **240**, 385–392.

47 B. Faure, G. Salazar-Alvarez and L. Bergstrom, *Langmuir*, 2011, **27**, 8659–8664.

48 J. Wang, Y. Sun, M. Yu, X. Lu, S. Komarneni and C. Yang, *J. Colloid Interface Sci.*, 2021, **589**, 378–387.

49 J. Ortega-Vinuesa, A. Martın-Rodrıguez and R. Hidalgo-Alvarez, *J. Colloid Interface Sci.*, 1996, **184**, 259–267.

50 S. Noskov, C. Scherer and M. Maskos, *J. Chromatogr. A.*, 2013, **1274**, 151–158.

51 X. Wang, N. Bolan, D. C. Tsang, B. Sarkar, L. Bradney and Y. Li, *J. Hazard. Mater.*, 2021, **402**, 123496.

52 A. P. Thompson, H. M. Aktulga, R. Berger, D. S. Bolintineanu, W. M. Brown, P. S. Crozier, P. J. in't Veld, A. Kohlmeyer, S. G. Moore, T. D. Nguyen *et al.*, *Comput. Phys. Commun.*, 2022, **271**, 108171.

53 G. Drazer, J. Koplik, A. Acrivos and B. Khusid, *Phys. Rev. Lett.*, 2002, **8924**, 4501.

54 G. Drazer, B. Khusid, J. Koplik and A. Acrivos, *Phys. Rev. Lett.*, 2005, **95**, 016102.

55 T. Yin, D. Shin, J. Frechette, C. E. Colosqui and G. Drazer, *Phys. Rev. Lett.*, 2018, **121**, 238002.

56 R. J. Good, *J. Adhes. Sci. Technol.*, 1992, **6**, 1269–1302.

57 A. Feng, B. J. McCoy, Z. A. Munir and D. Cagliostro, *Mater. Sci. Eng. A.*, 1998, **242**, 50–56.

58 T. Chau, W. Bruckard, P. Koh and A. Nguyen, *Adv. Colloid Interface Sci.*, 2009, **150**, 106–115.

59 S. E. Anachkov, I. Lesov, M. Zanini, P. A. Kralchevsky, N. D. Denkov and L. Isa, *Soft Matter*, 2016, **12**, 7632–7643.